ASTROBIOLOGY
Volume 18, Number 1, 2018

DOI: 10.1089/ast.2017.1650

Research Article

Transport-Induced Spatial Patterns of Sulfur Isotopes ($\delta^{34}S$) as Biosignatures

Muammar Mansor,[1,2] Khadouja Harouaka,[1,3] Matthew S. Gonzales,[1]
Jennifer L. Macalady,[1] and Matthew S. Fantle[1]

Abstract

Cave minerals deposited in the presence of microbes may host geochemical biosignatures that can be utilized to detect subsurface life on Earth, Mars, or other habitable worlds. The sulfur isotopic composition of gypsum ($CaSO_4 \cdot 2H_2O$) formed in the presence of sulfur-oxidizing microbes in the Frasassi cave system, Italy, was evaluated as a biosignature. Sulfur isotopic compositions ($\delta^{34}S_{V\text{-}CDT}$) of gypsum sampled from cave rooms with sulfidic air varied from −11 to −24‰, with minor deposits of elemental sulfur having $\delta^{34}S$ values between −17 and −19‰. Over centimeter-length scales, the $\delta^{34}S$ values of gypsum varied by up to 8.5‰. Complementary laboratory experiments showed negligible fractionation during the oxidation of elemental sulfur to sulfate by *Acidithiobacillus thiooxidans* isolated from the caves. Additionally, gypsum precipitated in the presence and absence of microbes at acidic pH characteristic of the sulfidic cave walls has $\delta^{34}S$ values that are on average 1‰ higher than sulfate. We therefore interpret the 8.5‰ variation in cave gypsum $\delta^{34}S$ (toward more negative values) to reflect the isotopic effect of microbial sulfide oxidation directly to sulfate or via elemental sulfur intermediate. This range is similar to that expected by abiotic sulfide oxidation with oxygen, thus complicating the use of sulfur isotopes as a biosignature at centimeter-length scales. However, at the cave room (meter-length) scale, reactive transport modeling suggests that the overall ∼13‰ variability in gypsum $\delta^{34}S$ reflects isotopic distillation of circulating H_2S gas due to microbial sulfide oxidation occurring along the cave wall-atmosphere interface. Systematic variations of gypsum $\delta^{34}S$ along gas flow paths can thus be interpreted as biogenic given that slow, abiotic oxidation cannot produce the same spatial patterns over similar length scales. The expression and preservation potential of this biosignature is dependent on gas flow parameters and diagenetic processes that modify gypsum $\delta^{34}S$ values over geological timescales. Key Words: Gypsum—Sulfur isotopes—Biosignature—Sulfide oxidation—Cave. Astrobiology 18, xxx–xxx.

1. Introduction

The martian subsurface is a prime target for future space missions with primary objectives focusing on the identification of life (Committee on an Astrobiology Strategy for the Exploration of Mars, 2007). Relative to the inhospitable conditions at the martian surface, the subsurface has a more stable temperature, can shield organisms from damaging ultraviolet radiation, and may contain liquid water critical to life. Subsurface mineral deposits formed in the presence of active microbial metabolisms may record the presence of life, thereby serving as targets for sample analysis missions. Interpretation of mineral-based biosignatures is, however, often complicated by competing signals from abiotic processes, as well as by post-deposition alteration (diagenesis) that overprints the original signature (Banfield *et al.,* 2001; Des Marais *et al.,* 2008). Additionally, from the standpoint of sampling in natural systems, there are added complications that stem from transport processes and the length scales over which biosignatures are expressed. Therefore, it is critical to understand whether a geochemical signature can be definitively attributed to life and how the expression and preservation potential of a given biosignature varies in nature.

To accomplish this goal, one approach is to investigate mineral-based biosignatures in Earth's subsurface. In particular, sulfidic caves on Earth that host extensive ecosystems in the absence of light (Sarbu *et al.,* 1996, 2000; Vlasceanu *et al.,* 2000; Boston *et al.,* 2006; Jones *et al.,* 2008) are promising analogues for potential life-hosting, subsurface systems on planets with inhospitable surfaces.

[1]Geosciences Department, Pennsylvania State University, University Park, Pennsylvania.
[2]Current address: Dept. of Geological Sciences, University of Texas at El Paso, El Paso, Texas.
[3]Department of Civil and Environmental Engineering, Rice University, Houston, Texas.

Sulfidic caves are formed by sulfuric acid speleogenesis, via the oxidation of hydrogen sulfide (H_2S) transported into the cave through groundwater. Hydrogen sulfide is degassed due to turbulent flow and oxidized above the water table to sulfuric acid by aerobic microbes such as *Acidithiobacillus thiooxidans* (Hose *et al.,* 2000; Macalady *et al.,* 2007; Jones *et al.,* 2011, 2014). The produced sulfuric acid dissolves limestone (Eq. 1), enlarges cavities, and subsequently forms gypsum deposits ($CaSO_4 \cdot 2H_2O$) that can accumulate to several centimeters' thickness on the cave wall (Hose *et al.,* 2000; Galdenzi and Maruoka, 2003; Jones *et al.,* 2015):

$$H_2SO_4 + CaCO_3 \rightarrow CO_2 + H_2O + Ca^{2+} + SO_4{}^{2-} \quad (1)$$

Massive deposits of gypsum have been found in both actively forming and inactive sulfidic caves as old as 10 million years (*e.g.,* Hill, 2000; Galdenzi and Maruoka, 2003; De Waele *et al.,* 2016).

Given that microbial H_2S oxidation is 10 to 10^5 faster relative to abiotic oxidation (Wilmot *et al.,* 1988; Buisman *et al.,* 1990; Luther *et al.,* 2011; Jones *et al.,* 2015), a geochemical tracer of microbial sulfur cycling may be expressed in gypsum. One such tracer is sulfur isotopes ($\delta^{34}S$). Compiled gypsum $\delta^{34}S$ values from several sulfidic caves showed tremendous variability, spanning a range of +5‰ to −13‰ relative to the presumed H_2S source (Table 1). Gypsum $\delta^{34}S$ values reflect the sulfate source, being consistently higher by about 1‰ (Raab and Spiro, 1991, and references therein). If microbial H_2S oxidation produces sulfate with a distinct isotopic composition compared to abiotic processes, gypsum $\delta^{34}S$ can be a target for biosignatures. Sulfate production via H_2S may be indirect and proceed through the formation and further oxidation of sulfur species of intermediate oxidation states such as thiosulfate, sulfite, and elemental sulfur with distinct isotopic fractionations. Thus, to use S isotopes as biosignatures, it is crucial to constrain the isotopic fractionation factor associated with microbial H_2S oxidation as well as the oxidation pathways in the cave system, alongside additional variability associated with the H_2S source isotopic composition and transport processes.

In this study, we evaluate the extent to which gypsum from the sulfidic Frasassi caves reflects the microbial H_2S oxidation known to be occurring in the system. Over 50 gypsum samples were collected and characterized for S isotopes and morphology. The data were used to constrain the apparent isotopic fractionation associated with aerobic microbial H_2S oxidation in this system. Coupled to reactive transport models that take into account H_2S gas flow, the different length scales at which microbial H_2S oxidation

Table 1. Summary of Sulfur Isotopic Data in Sulfidic Caves

Location	*Descriptions*	$\delta^{34}S_{H_2S}$ (‰)	$\delta^{34}S_{gypsum}$ (‰)	$\Delta^{34}S_{gypsum\text{-}H_2S}$ (‰)	$\delta^{34}S_{S0}$ (‰)	*Refs.*
Frasassi caves, Italy						
Ramo Sulfureo	Active, microbially rich	−15 to −17[a]	−11 to −24	+4 to −9	−17 to −19	1, 2, 3
Grotta Bella	Active, microbially rich	−11 to −16[b]	−14 to −23	+2 to −7	—	1
Laghi di Lucia	Active, microbially rich	−16[c]	−18 to −20	−2 to −4	—	2, 3
Pozzo dei Cristalli	Unclear	−15[a]	−8 to −10	+5 to +7	—	2, 3
Other cave rooms	Inactive or unclear	—	−8 to −16	—	—	2
Triponzo Spring, Italy	Active	−9[a]	−19 to −24	−10 to −15	—	2
Cueva de Villa Luz, Mexico	Active, microbially rich	−12[b]	−22 to −25	−10 to −13	−24 to −27	4
Cave-and-Basin Springs	Active	−7[a]	−5 to −12	+2 to −5	—	5
Borup Fiord Pass, Canada	Active. Glacier ''pipes'' feature	+9[a]	+7 to +14	+5 to −2	+8 to +14	6
Cerna Valley caves, Romania						
Diana	Active	+19 to +24[a]	+18 to +20	~0	—	7, 8
Despicatura	Active	+19 to +24[a]	+14 to +19	+5 to 0	—	8
Hercules	Active	+19 to +24[a]	+14	+5	—	8
Birzoni	Inactive	−14 to −23[a]	−23 to −28	+2 to −2	—	8
Great Salitrari, inner part	Inactive	−14 to −23[a]	−20 to −22	+3 to +5	—	8
New Mexico caves, USA						
Guadalupe Mountains	Inactive	—	−25 to +5	—	−15 to −25	9
Lechuguilla Cave	Inactive	—	−26	—	−21 to −26	10
Carlsbad Cavern	Inactive	—	−15 to −22	—	—	10
Corkscrew Cave, USA	Inactive	—	−8 to −10	—	—	11
Kraushöhle, Austria	Inactive	—	−16 to −23	—	—	12
Acqua Fitusa Cave, Italy	Inactive	—	−1 to +11	—	—	12
Grotte du Chat, France	Inactive	—	−9	—	—	12
Provalata Cave, Macedonia	Inactive	—	−2	—	—	12

(1) This study. (2) Galdenzi and Maruoka (2003). (3) Zerkle *et al.* (2016). (4) Hose *et al.* (2000). (5) van Everdingen *et al.* (1985). (6) Grasby *et al.* (2012). (7) Onac *et al.* (2009). (8) Onac *et al.* (2011). (9) Hill (2000). (10) Pisarowicz (1994). (11) Onac *et al.* (2007). (12) De Waele *et al.* (2016).

[a]Groundwater H_2S.

[b]H_2S gas.

[c]Average $\delta^{34}S$ of groundwater H_2S in Frasassi.

imparts variations in $\delta^{34}S$ of cave gypsum deposits are explored, yielding spatial patterns in $\delta^{34}S$ at the meter-length scales that can be recognized as biosignatures. A simple strategy for detecting biosignatures in ancient cave systems through systematic sampling of mineral deposits over meter-length scales is presented. The preservation potential of this biosignature is discussed in terms of gas flow variability and physical and chemical diagenesis.

2. Sampling Site

The Frasassi cave system in Italy (43.39 N, 12.96 E) is a large network of actively forming and older passages with an explored length of 25 km (Fig. 1a). Temperature fluctuations in the cave are small ($13 \pm 1°C$), and humidity is constantly near 100%. A recent study suggests that subaerial H_2S oxidation at Frasassi is more important for cave formation than subaqueous H_2S oxidation (Jones *et al.,* 2015). Limestone cave walls are actively dissolving, resulting in gypsum crusts along with small amounts of elemental sulfur (S(0)). Gypsum crystals display different textures, including a pasty mixture made up primarily of microcrystalline gypsum, dry wall crusts, and centimeter-sized euhedral needles (Galdenzi and Maruoka, 2003; Macalady *et al.,* 2007; Harouaka *et al.,* 2016). The gypsum deposits are often covered with acidic biofilms, including mucus-like ''snottites'' with pH <1.8 (Vlasceanu *et al.,* 2000; Galdenzi and Maruoka, 2003; Macalady *et al.,* 2007; Jones *et al.,* 2008, 2011, 2014). Snottites are dominated by the aerobic S-oxidizing species of *A. thiooxidans*, as well as smaller populations of *Acidimicrobium* and relatives of the archaeon taxon G-plasma (Vlasceanu *et al.,* 2000; Macalady *et al.,* 2007; Jones *et al.,* 2011, 2014). Snottite populations were shown to contain diverse forms of sulfide:quinone oxidoreductase (SQR) and sox genes implicated in sulfide oxidation (Jones *et al.,* 2011, 2014).

Two cave rooms were sampled in this study: Ramo Sulfureo and Grotta Bella (Fig. 1b–1c). Sample locations are near the water table above H_2S-degassing streams. In Grotta Bella, $H_2S(g)$ rises through several chimneys that begin at the water table approximately 8 m below. The $H_2S(g)$ concentration in the chimneys ranges between 3 and 8 ppmv (Jones, 2011). In comparison, $H_2S(g)$ concentrations at Ramo Sulfureo's sampling sites are higher, ranging from 3.4 to 25 ppmv and decreasing quickly away from the water table (Galdenzi and Maruoka, 2003; Macalady *et al.,* 2007; Galdenzi *et al.,* 2008; Jones *et al.,* 2008, 2011, 2014). Sulfur dioxide gas was not detected at either site (Jones *et al.,* 2011, 2014).

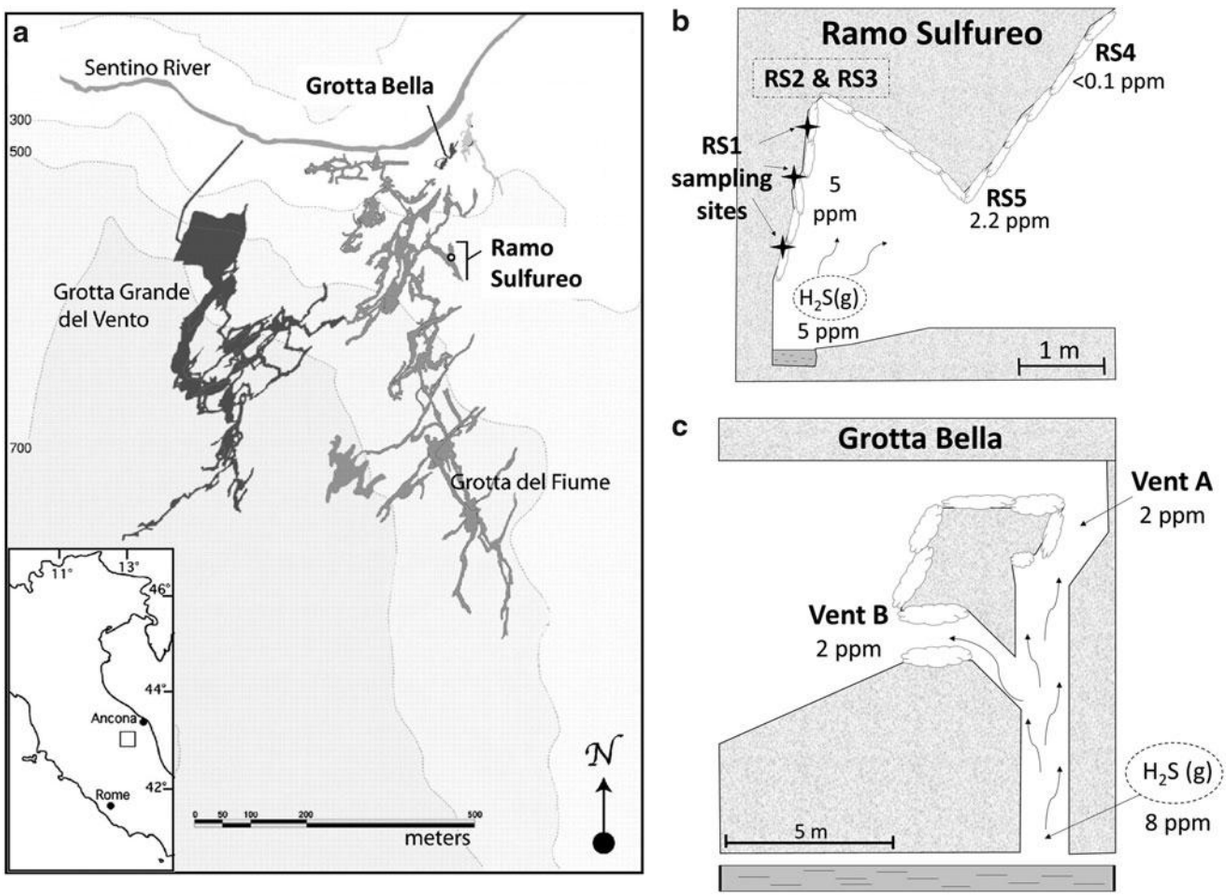

FIG. 1. (**a**) Map of the Frasassi cave system, modified from Macalady *et al.* (2006). Sampling locations in this study are in bold. (**b**) Schematic cross-sectional view of Ramo Sulfureo stream passage, depicting sampling sites RS1 to RS5. RS2 and RS3 are located downstream of site RS1. (**c**) Schematic cross-sectional view of Grotta Bella passage. $H_2S(g)$ rises from a chimney connected to the water table and out through two openings (vents A and B).

3. Materials and Methods

3.1. Field sampling

Gypsum and elemental sulfur deposits were collected with a clean spatula into acid-cleaned tubes prefilled with 90% isopropanol or 95% ethanol. Figure 1 shows sampling locations in Grotta Bella (GB) and Ramo Sulfureo (RS). In Grotta Bella, 21 samples were collected from areas within 2 m of H_2S-degassing chimneys. In Ramo Sulfureo, over 50 total samples were collected. Five different locations in Ramo Sulfureo (named RS1 to RS5) located within 5 m of the water table were extensively sampled (Fig. 1b). Gypsum minerals were collected as a function of height from the water table (RS1) or morphology (RS2, RS3, and RS4). At location RS5, soft gypsum crust about 2.5 cm thick was subsectioned by layers into nine approximately equal portions and analyzed separately. Additionally, four gypsum samples associated with visible, yellowish elemental sulfur deposits were collected from sites RS05 and RS07. At all collection sites, the pH of damp gypsum crusts or limestone walls was measured with pH strips.

H_2S(g) and SO_2(g) concentrations were measured with either a PGD2 portable gas detector (ENMET Corp., Ann Arbor, MI, USA), Draeger diffusion tubes (part # 6733091; 2.5 h equilibration time), or Draeger pump tubes (part # 6728041; Sugarland, TX, USA). Error in gas measurements is estimated to be up to 25%. At Grotta Bella, H_2S(g) was collected for isotopic analysis by using a 1 L gas syringe with a gas-tight valve connected to Tygon tubing. The air sample was directly pumped into 100 mL of 20% zinc acetate solution until the solution became cloudy, indicating the precipitation of zinc sulfide. The precipitates were pelleted by centrifugation at 6000*g* for 15 min. The supernatants were removed, and the pellets were converted to Ag_2S by the addition of 1 mL 10% $AgNO_3$. Precipitated Ag_2S particles were then pelleted by centrifugation as above, and the supernatants were removed.

3.2. Laboratory analysis: Gypsum and elemental sulfur

Quantitative analysis of gypsum crystal morphology was achieved by measuring aspect ratios (length/width of a crystal) by imaging via a dissecting microscope (for large gypsum needles) or scanning electron microscopy equipped with an energy dispersive spectroscopy (EDS) detector (FEI Quanta 200 ESEM). For microcrystalline gypsum and coarse-grained (wall crust) samples, aspect ratios of over 50 individual crystals were averaged to obtain the bulk aspect ratio of the sample, with typical 1 SD of <1.8. Aspect ratios of gypsum needles were averaged from varying numbers of crystals due to sample limitation, ranging from one (single crystal) to 50.

Organic carbon contents were measured on a C/S analyzer (LECO Corporation, MI, USA). Gypsum samples were dried at 60°C and powdered before being weighed into the instrument. Samples containing observable calcite under scanning electron microscope were excluded from measurements. Blank tests on laboratory grade $CaSO_4$ (Alfa Aesar) were performed to check for carbon contamination from ethanol or isopropanol used during sampling. Untreated and ethanol-treated laboratory $CaSO_4$ yielded organic carbon values within measurement error of ±0.04 wt %.

For S isotopic analyses, gypsum samples from Grotta Bella were briefly vortexed and sonicated in isopropanol for 10 min. Samples were then centrifuged at 4000*g* for 10 min. A dark brown substance, likely composed of organic materials and clay particles, separated out into the solution or settled at the top of the gypsum pellet. This substance was removed by pipetting. The samples were centrifuged and pipetted from the top repeatedly until the dark substance was no longer visible and only pure gypsum remained.

Gypsum samples from Ramo Sulfureo were powdered and dissolved overnight in 5 mL 5 *N* HCl with continuous shaking. Residual solids were pelleted at 6000*g* for 20 min. Supernatants containing dissolved sulfate were transferred to clean tubes and precipitated as $BaSO_4$ by the addition of 1 mL 1 *M* $BaCl_2$ solution. Precipitated $BaSO_4$ was pelleted by centrifugation at 6000*g* for 20 min. The supernatant was removed, and the remaining $BaSO_4$ was washed twice with H_2O.

Elemental sulfur particles were separated from gypsum by repeated dissolution of gypsum in 5 *N* HCl. The samples were then extensively washed in water by repeated centrifugation. Brown residues that settled to the top of the yellow elemental sulfur layer were removed by resuspension and pipetting until only pure elemental sulfur remained (confirmed by measuring sulfur weight percent via the C/S analyzer).

3.3. Experimental determination of isotopic fractionation

Three laboratory experiments were conducted to determine fractionation during (1) microbial S(0) oxidation to sulfate and (2) gypsum precipitation at acidic pH. In the first experiment, triplicate cultures of *A. thiooxidans* strain GB30-2c, isolated from gypsum crust in the Grotta Bella cave room (Jones *et al.,* 2016), were grown on a shaker table at room temperature in defined mineral medium containing 3 g/L KH_2PO_4, 0.4 g/L $MgCl_2 \cdot 6H_2O$, 0.25 g/L $CaCl_2 \cdot 2H_2O$, 0.08 g/L NH_4Cl, and supplemented with 10g/L S(0). Elemental sulfur was presterilized by autoclaving at 100°C for 30 min on 3 consecutive days. Initial pH of the medium was 4.2. Sampling and analyses were performed weekly for 3 weeks. Cell concentrations were counted with a hemacytometer, pH values were determined with pH strips, and sulfate concentrations were determined by anion chromatography (Dionex ICS-2500) on 0.2 μm filtered samples. For isotopic analysis, sulfate was precipitated as $BaSO_4$ by the addition of $BaCl_2$, which was then centrifuged and washed repeatedly with MQ water as described above to >95% purity. Initial and final S(0) particles were pelleted by centrifugation at 8000*g* for 20 min. After removal of the supernatant, S(0) was treated with 12.5 mg/mL lysozyme and 1% sodium dodecyl sulfate (SDS) to remove cell materials (Bosshard *et al.,* 2000; Zerkle *et al.,* 2009). The treated S(0) was pelleted as before and washed at least three times with MQ water to remove any traces of SDS.

In the second experiment, gypsum was precipitated abiotically at pH 5.5. Experimental procedures and detailed geochemical data for this experiment were described previously (Harouaka *et al.,* 2014). Briefly, $CaCl_2 \cdot 2H_2O$ and Na_2SO_4 stock solutions were mixed together in a batch reactor to precipitate gypsum over a range of saturation states. Gypsum was allowed to precipitate until dissolved Ca concentrations reached a stable value as monitored by analysis of solution aliquots via inductively coupled plasma–atomic emission spectroscopy. The crystals were collected after filtration through a 0.45 μm PVDF filter paper. In the third experiment,

gypsum was precipitated in a mineral medium containing S(0) (final pH 1.3–1.6) and 50 m*M* Ca either in the presence or absence of *A. thiooxidans* (Series 1 experiments; Harouaka *et al.,* 2016). In these second and third experiments, the S isotopic compositions of the final dissolved sulfate (precipitated as $BaSO_4$) and gypsum were analyzed.

3.4. Measurements of S isotopic compositions ($\delta^{34}S$) and isotopic notations

Sulfur isotopic analyses of air-dried and powdered Ag_2S, $CaSO_4$, $BaSO_4$, and S(0) were conducted via elemental analysis–isotopic ratio mass spectrometry either at the Carnegie Institution of Washington, Pennsylvania State University, or the SIRFER facility at the University of Utah. About 0.05–1 mg of powdered samples was placed into tin tubes, mixed with excess V_2O_5, and combusted at 1000–1200°C to produce SO_2, which was then measured by the spectrometer. All isotope measurements are expressed in delta notation ($\delta^{34}S$; Eq. 2) relative to Vienna Canyon Diablo Troilite (V-CDT) isotopic standard:

$$\delta^{34}S_{sample} = \left[\left({}^{34}S/{}^{32}S \right)_{sample} / \left({}^{34}S/{}^{32}S \right)_{V\text{-}CDT} - 1 \right] \cdot 1000 \quad (2)$$

Isotopic standards were used to construct calibration curves for linear and two-point corrections. International standards used were NBS-127, NBS-123, IAEA-S-1, and IAEA-S-3 with $\delta^{34}S$ values of +20.3, +17.1, –0.3, and –32.3‰, respectively (IAEA, 1995). In-house standards include lab-prepared GFS barite ($\delta^{34}S = -3.2$‰, Watanabe *et al.,* 2009), methionine ($\delta^{34}S = -6.2$‰), and natural barite from the Fig Tree group, Barberton, South Africa ($\delta^{34}S = +4.1$‰). External reproducibility was < ±0.5‰ (1 SD) for all samples, as determined by the analysis of standards and replicate samples over multiple analytical sessions.

We denote the intrinsic fractionation factor associated with a process using alpha (α) notation, where the subscripts P and R stand for product and reactant, respectively:

$$\alpha_{P/R} = \frac{1000 + \delta^{34}S_P}{1000 + \delta^{34}S_R} \quad (3)$$

In systems where α is not known, or isotopic expression is the result of multiple processes as is typical for natural systems, the apparent isotopic fractionation between two phases can instead be written in terms of the capital delta (Δ) notation, where the subscripts a and b represent distinct phases:

$$\Delta^{34}S_{a\text{-}b} = \delta^{34}S_a - \delta^{34}S_b \quad (4)$$

4. Results

4.1. Field data

Description and analytical results for all samples are presented in Table 2. The pH values of all gypsum crusts were <2.5. Concentrations of H_2S(g) ranged between 1.5 and 5 ppmv, with the exception of site 4 in the Ramo Sulfureo cave room (RS4) where H_2S(g) was below the detection limit (<0.1 ppmv). Sulfur dioxide gas was never detected (<0.1 ppmv). At Grotta Bella, the concentration of H_2S(g) in the chimney was 8 ppmv just above the water table and was constant, within error, to 7.8 m above the water table. At the top of the chimney (vent A), 8 m above the water table, H_2S(g) concentration was 2 ppmv. Measured $\delta^{34}S$ values of H_2S(g) at vent A and just above the water table were –16.5 and –11‰, respectively. At vent B in Grotta Bella, the H_2S(g) concentration was 2 ppmv with a $\delta^{34}S$ value of –10.2‰.

4.2. Grain morphology

Variants of gypsum morphologies were observed through the naked eye as well as by microscopy, which can be classified into soft microcrystalline gypsum aggregates, coarser-grained wall crusts, small needles, and large needles. Microcrystalline gypsum aggregates are the most prevalent form of gypsum in the cave and are composed of <30 μm long crystals (Fig. 2a). Wall crust gypsum tends to show larger variations in terms of crystal sizes, ranging from 10 to 2000 μm long crystals (Fig. 2b). Needles are common but less prevalent than microcrystalline gypsum and wall crusts. At Ramo Sulfureo, small needles between 0.1 and 1 cm long (Fig. 2c) are found near the water table, often in association with snottite biofilms.

Scanning electron microscopy observations of snottite surfaces revealed gypsum minerals embedded within a biofilm matrix (Fig. 2d). Elemental sulfur particles (Fig. 2e) and amorphous organic matter were found in association with some gypsum samples. Aspect ratios for all gypsum crystals ranged between 1.8 and 22.7 (Table 2). We classified the gypsum minerals into two main types based on aspect ratios: microgypsum (including wall crusts; aspect ratios between 1.8 and 4.4) and needles (aspect ratios between 7 and 23).

4.3. Sulfur isotopic compositions of gypsum and elemental sulfur

The $\delta^{34}S$ of microgypsum, needles, and elemental sulfur ranged from –15 to –24‰, –12 to –19‰, and –17 to –19‰, respectively (Fig. 3; Table 2). Gypsum samples collected within 10 cm of one another showed $\delta^{34}S$ variations of up to 8.5‰, with microgypsum typically showing lower values relative to needles (Fig. 4). Physically separated microgypsum around needles also had lower $\delta^{34}S$ values (–19.2 ± 0.3‰) relative to the needles (–17.0 ± 0.1‰) (site RS2, $n = 2$). Elemental sulfur particles were isotopically similar to associated gypsum, ranging from being 0.2‰ higher to 2.2‰ lower (site RS05 and RS07, $n = 4$).

At site RS5 where gypsum was sampled by depth, $\delta^{34}S$ values ranged between –15.7 and –23.9‰ with no systematic variation with distance from the limestone cave wall. Interestingly, $\delta^{34}S$ values decreased with height at site RS1, with average values of –19.5 ± 1.4, –21.0 ± 1.0, and –23.6 ± 0.5‰ at 1.2, 2.0, and 2.6 m height from the water table, respectively (Fig. 5).

4.4. Experimental results

During growth on elemental sulfur, *A. thiooxidans* produces sulfuric acid as the sole product. Cell density increased from $1 \cdot 10^6$ to $2.5 \cdot 10^8$ cells/mL over 3 weeks, with a concurrent increase in dissolved sulfate (up to 60 m*M*) and decrease in pH from 4.2 to 1.3. Abiotic controls did not show any sulfate production. The $\delta^{34}S$ of sulfate and elemental sulfur in the cultures at the end of the incubation were within ±0.5‰ relative to initial elemental sulfur (Supplementary Table S1; Supplementary Data

Table 2. Description and Analytical Results for All Samples

Sample	*Description*	*Aspect ratio (length/width)*	*$\delta^{34}S$ (‰)*	*Org C (wt %)*	*[$H_2S(g)$] (ppmv)*	*Height from water table (m)*	*Lateral distance from H_2S source (m)*
GB2009							
OP-1	Microgypsum	2.0 ± 1.0	−20.4	—	—	—	—
OP-2	Small needles	7.2 ± 4.5	−18.5	—	—	—	—
OP-3	Wall crust gypsum	4.4 ± 1.1	−21.2	—	—	—	—
OP-4	Large needles	11.6 ± 5.2	−14.2	—	—	—	—
GB2011							
H_2S-A1	H_2S gas at chimney A	—	−11.0	—	8.0	0.4	0.00
H_2S-A2	H_2S gas at chimney A	—	—	—	6.4	4.0	0.00
H_2S-A3	H_2S gas at chimney A	—	—	—	7.7	5.0	0.00
H_2S-A4	H_2S gas at chimney A	—	—	—	7.5	6.0	0.00
H_2S-A5	H_2S gas at chimney A	—	—	—	8.8	6.5	0.00
H_2S-A6	H_2S gas at chimney A	—	—	—	9.8	7.0	0.00
H_2S-A7	H_2S gas at chimney A	—	—	—	8.4	7.2	0.00
H_2S-A8	H_2S gas at chimney A	—	—	—	7.0	7.4	0.00
H_2S-A9	H_2S gas at chimney A	—	—	—	8.4	7.6	0.00
H_2S-A10	H_2S gas at chimney A	—	—	—	5.6	7.8	0.00
H_2S-A11	H_2S gas at chimney A	—	−16.5	—	2.0	8.0	0.00
H_2S-B1	H_2S gas at chimney B	—	−10.2	—	2.0	8.0	0.00
001	Microgypsum	—	−23.2	—	2.7–5.0	8.0	—
250	Microgypsum	—	−21.9	—	2.7–5.0	8.0	—
537	Microgypsum	—	−22.5	—	2.7–5.0	8.0	—
591	Microgypsum	2.0 ± 0.8	−18.5	—	2.7–5.0	8.0	0.02
599	Microgypsum	2.4 ± 1.3	−18.4	—	2.7–5.0	8.0	0.12
603	Microgypsum	2.4 ± 1.3	−20.4	—	2.7–5.0	8.0	0.22
611	Microgypsum	2.5 ± 1.0	—	—	2.7–5.0	8.0	0.30
629	Microgypsum-needles mixture	2.3 ± 1.3	−18.9	—	2.7–5.0	8.0	0.52
629N	Microgypsum-needles mixture	—	−19.5	—	2.7–5.0	8.0	0.52
637	Microgypsum-needles mixture	3.5 ± 2.3	−19.5	—	2.7–5.0	8.0	1.10
647	Needles, 1.2–1.5 cm long	10.6 ± 1.2	−17.7	—	2.7–5.0	8.0	0.06
655	Microgypsum	2.8 ± 1.5	—	—	2.7–5.0	8.0	1.70
685	Microgypsum	1.9 ± 0.9	—	—	2.7–5.0	8.0	0.64
688	Wall crust gypsum	1.9 ± 0.8	—	—	2.7–5.0	8.0	0.79
691	Wall crust gypsum	—	−22.7	—	2.7–5.0	8.0	—
739	Microgypsum	—	−20.4	—	2.7–5.0	8.0	—
743	Wall crust gypsum	2.0 ± 1.8	—	—	2.7–5.0	8.0	—
RS05							
2G	Brownish microgypsum with snottites	—	−16.5	—	—	—	—
2S	S(0) around snottites	—	−18.7	—	—	—	—
4G	Microgypsum	—	−17.4	—	—	—	—
4S	S(0) around microgypsum	—	−18.7	—	—	—	—
RS07							
21G	Microgypsum	—	−17.5	—	—	—	—
21S	S(0) around microgypsum	—	−17.3	—	—	—	—
22G	Microgypsum	—	−17.8	—	—	—	—
22S	S(0) around microgypsum	—	−17.9	—	—	—	—
RS1							
1.2m-A	Microgypsum	2.3 ± 1.0	−17.1	0.35	5.0	1.2	0.00
1.2m-B	Microgypsum	2.2 ± 1.1	−20.5	0.51	5.0	1.2	0.00
1.2m-C	Microgypsum	2.0 ± 0.8	−20.6	0.55	5.0	1.2	0.00
1.2m-D	Microgypsum	2.4 ± 1.1	−19.7	—	5.0	1.2	0.00
2m-A	Dry microgypsum	3.1 ± 1.8	−21.4	1.41	5.0	1.2	0.00
2m-B	Wet microgypsum	1.8 ± 0.8	−21.0	0.28	5.0	2.0	0.00
2m-C	Microgypsum	2.0 ± 1.0	−20.8	0.69	5.0	2.0	0.00
2m-C2	Microgypsum	2.0 ± 0.9	−22.3	0.70	5.0	2.0	0.00
2m-D	Microgypsum	2.5 ± 1.3	−19.3	1.39	5.0	2.0	0.00
2.6m-A	Microgypsum	2.0 ± 0.9	−24.2	0.15	5.0	2.6	0.00
2.6m-B	Microgypsum	1.8 ± 0.7	−23.4	0.41	5.0	2.6	0.00
2.6m-C	Microgypsum	2.1 ± 0.9	−23.9	0.61	5.0	2.6	0.00
2.6m-D	Dry microgypsum	2.1 ± 0.8	−22.9	—	5.0	2.6	0.00

(*continued*)

Table 2. (Continued)

Sample	*Description*	*Aspect ratio (length/width)*	*$\delta^{34}S$ (‰)*	*Org C (wt %)*	*$[H_2S(g)]$ (ppmv)*	*Height from water table (m)*	*Lateral distance from H_2S source (m)*
RS2							
1	Microgypsum around needles	3.4 ± 1.7	—	—	1.5	1.6	0.00
1N	Needles, 0.2–0.4 cm long	12.2 ± 4.7	—	—	1.5	1.6	0.00
2	Microgypsum around needles	3.3 ± 1.6	−19.5	—	1.5	1.6	0.00
2N	Needles, 0.15–0.45 cm long	11.0 ± 5.2	−17.1	—	1.5	1.6	0.00
3	Microgypsum around needles	3.4 ± 2.7	−18.9	—	1.5	1.6	0.00
3N	Needles, 0.1–0.3 cm long	10.5 ± 5.4	−16.9	—	1.5	1.6	0.00
4	Wet microgypsum	2.9 ± 1.4	−21.9	0.60	1.5	1.6	0.00
5	Wet microgypsum	2.0 ± 0.8	−22.1	0.50	1.5	1.6	0.00
6	Wet microgypsum	2.3 ± 1.2	−23 ±	0.77	1.5	1.6	0.00
7	Microgypsum	2.2 ± 1.4	−20.6	0.76	1.5	1.6	0.00
8	Microgypsum	2.7 ± 1.6	−22.8	—	1.5	1.6	0.00
9	Microgypsum	3.3 ± 1.4	−22.2	1.19	1.5	1.6	0.00
RS3							
1	Needle, 1.4 cm long	22.1	—	—	4.0	2.1	0.00
3	Needles, 0.4–1.2 cm long	22.7 ± 10.4	—	—	4.0	2.1	0.00
RS4							
1	Needle, 2.4 cm long	11.8	−14.2	0.41	<0.1	4.0	4.00
2	Needle, 3 cm long	14.2	−11.9	0.18	<0.1	4.0	4.00
3A	Needle, 2.3 cm long	8.00	−16.1	0.47	<0.1	4.0	4.00
3B	Needle, 2.0 cm long	12.5	−18.0	0.78	<0.1	4.0	4.00
4	Needle, 2.7 cm long	7.3	−18.4	0.60	<0.1	4.0	4.00
4B	Needle, 2.1 cm long	10.9	−18.5	0.67	<0.1	4.0	4.00
5	Needles, 0.1–0.5 cm long	9.8 ± 5.6	—	—	<0.1	4.0	4.00
6	Needles, 0.3–0.7 cm long	12.6 ± 3.6	−15.7	—	<0.1	4.0	4.00
8	Needles, 0.3–0.7 cm long	10.8 ± 4.6	−18.9	—	<0.1	4.0	4.00
9	Wet microgypsum	1.6 ± 0.9	−20.3	0.06	<0.1	4.0	4.00
10	Dry microgypsum	2.2 ± 1.1	−17.5	0.27	<0.1	4.0	4.00
11	Wall crust gypsum	3.8 ± 1.5	−18.2	1.16	<0.1	4.0	4.00
12	Wall crust gypsum	2.4 ± 1.6	−20.0	0.50	<0.1	4.0	4.00
RS5							
1	Microgypsum, outermost crust	2.1 ± 1.0	−17.7	—	4.5	1.8	2.20
2	Microgypsum	2.2 ± 0.9	−22.5	0.45	4.5	1.8	2.20
3	Microgypsum	2.0 ± 0.8	−22.5	0.83	4.5	1.8	2.20
4	Microgypsum	2.2 ± 0.9	−19.9	0.49	4.5	1.8	2.20
5	Microgypsum	2.1 ± 1.0	−15.7	0.40	4.5	1.8	2.20
6	Microgypsum	2.1 ± 0.9	−21.9	0.35	4.5	1.8	2.20
7	Microgypsum	1.9 ± 0.7	−23.9	—	4.5	1.8	2.20
8	Microgypsum	2.1 ± 0.8	—	0.38	4.5	1.8	2.20
9	Microgypsum, innermost crust	2.2 ± 1.0	−23.1	0.27	4.5	1.8	2.20

are available at http://online.liebertpub.com/doi/suppl/10.1089/ast.2017.1650), suggesting negligible fractionation during elemental sulfur oxidation to sulfate.

Gypsum crystals precipitated abiotically at pH 5.5 were 0.2‰ lower to 1.7‰ heavier relative to dissolved sulfate. Similarly, gypsum precipitated in the presence or absence of *A. thiooxidans* at pH 1.6 were between 0.1 and 1.2‰ heavier relative to dissolved sulfate. On average, the fractionation associated with gypsum precipitation is approximately +1‰.

5. Discussion

5.1. Comparison of isotopic effects due to microbial and abiotic H_2S oxidation at centimeter sampling scale

With the aim of evaluating the utility of gypsum $\delta^{34}S$ as biosignatures, it is crucial that we constrain the observed isotopic fractionation from active microbial H_2S oxidation in the caves and compare it to the fractionation expected solely from abiotic oxidation. Sulfate (in the form of gypsum) is the major end product of H_2S oxidation, with elemental sulfur being present only on small sections of the cave wall. Other products of H_2S oxidation such as thiosulfate and sulfite are expected to be minor or rapidly converted to sulfate under acidic conditions (Davis, 1958; Zhang and Millero, 1991; Kamyshny *et al.,* 2014) characteristic of the cave wall (pH<2.5). Thus, direct microbial H_2S oxidation to sulfate is likely the major pathway for sulfate production in this system.

In Frasassi, gypsum $\delta^{34}S$ varies from 4‰ higher to 9‰ lower relative to either H_2S in the groundwater or H_2S gas in the air (Fig. 3). This isotopic variation most likely reflects the combined effects of variation in $\delta^{34}S$ values of the H_2S source, microbial H_2S oxidation, and distillation effects as the H_2S

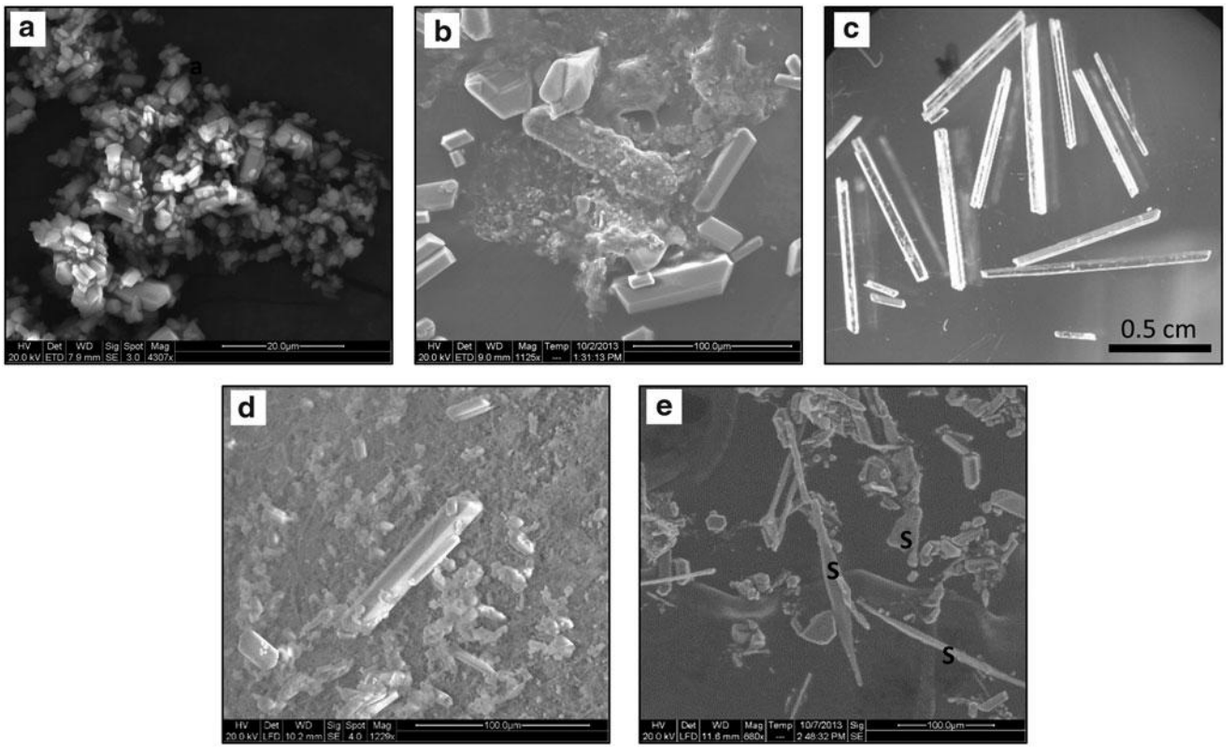

FIG. 2. (**a**) Scanning electron microscopic (SEM) image of microcrystalline gypsum aggregates. (**b**) SEM image of wall crust gypsum associated with amorphous organic matter. The presence of organic matter was confirmed using EDS. (**c**) Light microscopic image of gypsum needles. (**d**) SEM image of gypsum minerals on snottite surface. (**e**) SEM image of elemental sulfur (marked by ''S'') among gypsum minerals as confirmed using EDS.

source becomes depleted. In comparison, microbial oxidation of elemental sulfur to sulfate and subsequent gypsum precipitation will produce negligible isotopic fractionation, as suggested by laboratory experiments and field data from gypsum associated with elemental sulfur (site RS05 and RS07).

In terms of the H_2S source, long-term $\delta^{34}S$ monitoring of groundwater sulfide in Ramo Sulfureo (Zerkle *et al.,* 2016) coupled to consideration of fractionation during sulfide speciation (H_2S and HS^-) and volatilization/solubilization processes suggest a maximum variability of 3‰ to be imparted to

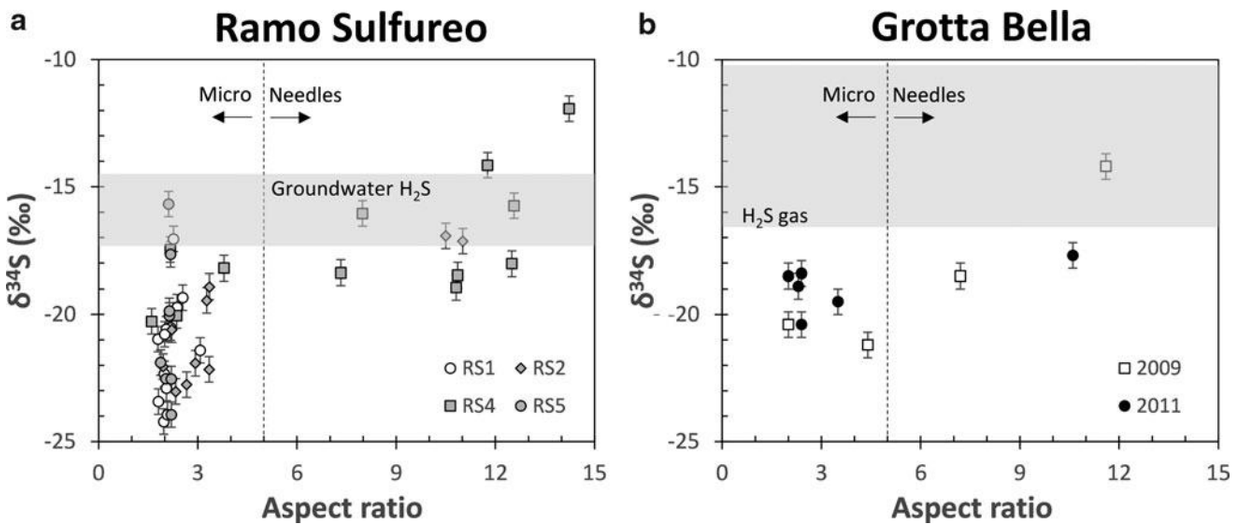

FIG. 3. Gypsum $\delta^{34}S$ values as a function of crystal aspect ratios at (**a**) Ramo Sulfureo and (**b**) Grotta Bella. Vertical line marks the approximate cutoff between microgypsum (aspect ratio < 5) and needles (aspect ratio > 5). Shaded horizontal box in (a) represents the $\delta^{34}S$ range of groundwater H_2S at Ramo Sulfureo (Galdenzi and Maruoka, 2003; Zerkle *et al.,* 2016). Shaded horizontal box in (b) represents the $\delta^{34}S$ range of H_2S gas at Grotta Bella (this study).

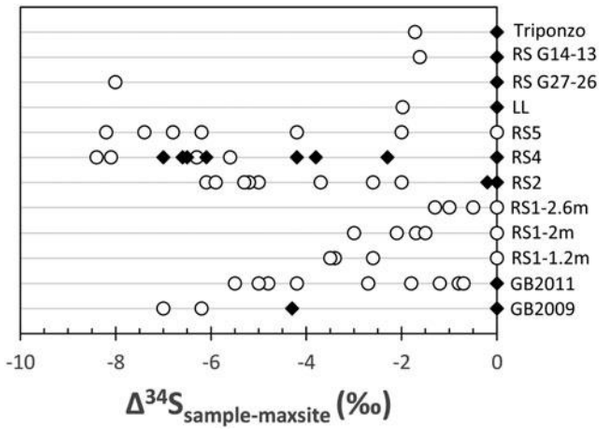

FIG. 4. $\Delta^{34}S$ values of gypsum relative to the maximum gypsum $\delta^{34}S$ value at each site. At sites where needles (◆) and microgypsum (○; including wall crusts) co-occur, microgypsum crystals are isotopically depleted relative to needles. Maximum range in $\delta^{34}S$ values of gypsum at each site is about 8.5‰. Data for samples LL, RS G27-26, RS G14-13, and Triponzo are from Galdenzi and Maruoka (2003).

gypsum $\delta^{34}S$ (Supplementary Discussion). Intriguingly, we found a 6‰ variation for H_2S gas sampled on the same day from various locations within Grotta Bella. This range cannot be explained by the aforementioned processes and is most likely caused by distillation effects during oxidation,

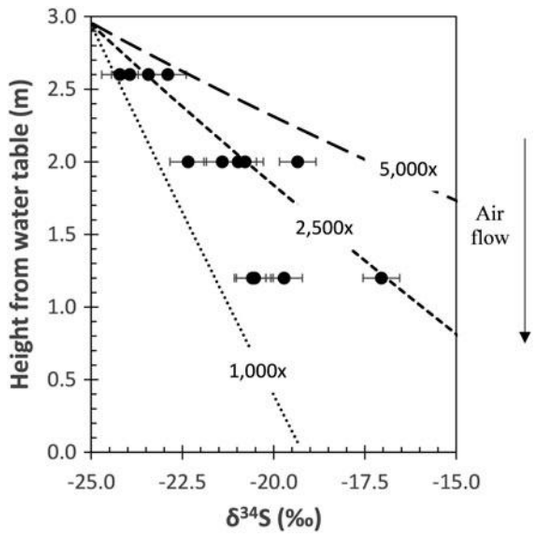

FIG. 5. Variations of gypsum $\delta^{34}S$ (black circles) as a function of height at location RS1. The two parameters are strongly correlated, with $R^2 = 0.67$. Different dashed lines denote sulfate $\delta^{34}S$ as a function of height based on 1D modeling results using different oxidation rates (relative to abiotic oxidation rate) with $\alpha_{oxi} = 0.992$. $H_2S(g)$ source at the top is assumed to have a $\delta^{34}S$ value of −17‰, which is similar to the minimum groundwater H_2S $\delta^{34}S$ at Ramo Sulfureo. H_2S oxidation rate is constrained to be between 1000 and 5000× faster relative to abiotic rate, indicating the spatial pattern is a type of biosignature for S-oxidizing microbes.

as suggested by large $H_2S(g)$ concentration differences within cave rooms (Fig. 1). Thus, we cannot assume a homogenous $\delta^{34}S$ value for H_2S gas that reaches microbial communities located on different parts of the cave wall. Upon oxidation, laboratory studies with *A. thiooxidans* suggest that the produced sulfate will have $\delta^{34}S$ values that are 6–18‰ lower relative to H_2S (Kaplan and Rafter, 1958; Kaplan and Rittenberg, 1964). The large isotopic effects are, however, measured when sulfate is the minor reaction product, have never been reproduced, and therefore may not apply to the cave system.

To circumvent these uncertainties, we therefore attempt to directly determine the apparent isotopic fractionation ($\Delta^{34}S_{SO_4\text{-}H_2S}$) due to microbial H_2S oxidation in the cave system by comparing the isotopic range of gypsum collected within small areas (<10 cm apart) of the cave walls. Up to 8.5‰ variations in gypsum $\delta^{34}S$ were observed, with needles having higher values compared to microgypsum by 2‰ on average (Fig. 4). We interpret these differences to reflect varying rates and extent of H_2S oxidation on needles relative to microgypsum (Galdenzi and Maruoka, 2003). The highest oxidation rate is expected around needles covered with dense microbial biofilms (snottites) in comparison to sparser populations around microgypsum crusts (Hose and Macalady, 2006; Macalady *et al.,* 2007; Jones *et al.,* 2011). Assuming control of $\delta^{34}S$ by distillation effects, the $\delta^{34}S$ of gypsum needles should be most similar to the original $\delta^{34}S$ of the H_2S source due to mass balance consideration. Our data then suggest that the apparent isotopic fractionation during microbial H_2S oxidation to sulfate (either directly or through elemental sulfur intermediate) varies from 0 to −8.5‰, and up to −9.5‰ if the +1‰ fractionation during gypsum precipitation is considered. The apparent fractionation determined for microbial oxidation in the cave system ($\Delta^{34}S_{SO4\text{-}H2S} = 0$ to −8.5‰) is at the more positive end of those determined from the 1960s experiments for *A. thiooxidans* (−6 to −18‰; Kaplan and Rafter, 1958; Kaplan and Rittenberg, 1964) and overlaps with results from culture experiments using anaerobic, chemotrophic microbes (−1.3 to −4.3; Poser *et al.,* 2014) that utilized similar H_2S oxidation pathways as *A. thiooxidans* (Jones *et al.,* 2011, 2014).

More importantly, we can compare the measured gypsum $\delta^{34}S$ to values expected from abiotic H_2S oxidation. Through abiotic oxidation experiments, Fry *et al.* (1988) showed that sulfate is expected to be on average 5‰ lower relative to the H_2S source, as calculated from isotopic mass balance using the measured $\delta^{34}S$ of residual H_2S. Multiple reaction products were also formed in the aforementioned experiments with distinct isotopic compositions. Thus, applying the experimentally determined fractionation to natural systems is difficult without knowing the proportion of reaction products. We therefore assume that sulfate will be the dominant product of abiotic H_2S oxidation in the cave system and that the average isotopic effect of −5‰ is representative of this reaction. With these assumptions, the measured gypsum $\delta^{34}S$ values are quite similar to those expected from abiotic H_2S oxidation (range of −1.8 to −7.3‰; mean = −5‰). Overall, the $\delta^{34}S$ values of actively forming gypsum at the centimeter scale cannot be used to distinguish between biological and abiotic H_2S oxidation with confidence and are ambiguous as biosignatures.

5.2. Impact of transport processes on the isotopic expression of microbial H_2S oxidation at the cave room scale

In Frasassi, the $\sim 13‰$ variation in gypsum $\delta^{34}S$ cannot be fully explained by microbial H_2S oxidation and $\delta^{34}S$ variation in groundwater sulfide. Additional processes, potentially related to isotopic fractionation of H_2S in the gas phase, are required to explain the isotopic variation. Interestingly, the $\delta^{34}S$ values of microgypsum and $H_2S(g)$ exhibit 5–6‰ variations with height above the water table (Fig. 5). Thus, we hypothesize that variations in isotopic values of gypsum at the cave room scale may be primarily a function of $H_2S(g)$ transport in tandem with isotopic distillation during microbial oxidation.

Convection and diffusion are two possible transport processes for $H_2S(g)$ in a cave system. Isotopic effects on $H_2S(g)$ will depend on which is dominant, as diffusion can fractionate while convection does not (Chanton, 2005). In the cave, gas convection is expected to dominate over diffusion due to temperature-driven air currents (see Supplementary Discussion). To visualize these air currents, we utilize Energy2D, a visual simulator that couples physical equations of heat transfer with fluid dynamics (Supplementary Materials; Xie, 2012). The simulations show that even with small temperature differences observed in Frasassi (<1°C), air convection is significant at the scale of a cave room. In Ramo Sulfureo, stable convection cells on the order of 3 m in diameter developed in the model simulations (Fig. 6). Passive tracers in Energy 2D simulations suggest that $H_2S(g)$ molecules released from the stream will concentrate mainly in the first convection cell above the stream surface. This is consistent with our data, which show a constant concentration of $H_2S(g)$ near the stream (~ 5 ppm) that decreases significantly over ~ 4 m to <0.1 ppm in Ramo Sulfureo. In contrast, the Grotta Bella cave room has a different geometry, which results in substantially different gas flow patterns. Temperature gradients between the bottom water and wall ceiling result in convection that is driven vertically upward through narrow chimneys in Grotta Bella. Thus, gas flow pattern is expected to differ considerably among different cave rooms due to geometrical variations and temperature gradients.

Since convection controls $H_2S(g)$ transport in the cave system, the transport process itself does not have an effect on the isotopic composition of $H_2S(g)$. Thus, chemical reactions between circulating H_2S gas and water films on the cave walls are likely the primary influence on the isotopic variability in gypsum. Specifically, we hypothesize that (1) isotopic exchange between $H_2S(g)$ and aqueous H_2S in water films ($H_2S(aq)$) and/or (2) subsequent oxidation of aqueous H_2S to sulfate may lead to the expression of isotopic distillation effects at meter-length scales. At equilibrium, the $\delta^{34}S$ of $H_2S(aq)$ will be 1‰ higher than $H_2S(g)$ at 13°C (Czarnacki and Hałas, 2012 and references therein), which will leave the convecting $H_2S(g)$ isotopically lighter. Meanwhile, the oxidation of H_2S to sulfate can generate isotopically light sulfate ($\alpha_{oxi} = 0.995$ assumed for abiotic oxidation, Fry *et al.,* 1988; $\alpha_{oxi} = 0.992$ assumed for microbial oxidation based on gypsum $\delta^{34}S$ variation at the centimeter scale), which will leave the residual $H_2S(aq)$ and $H_2S(g)$ isotopically heavy. To evaluate the extent to which these reactions can influence $\delta^{34}S$ of cave gypsum, we constructed a 1D model in CrunchTope (Steefel *et al.,* 2014) that simulates a 3 m air column in continuous contact with a cave wall that is saturated with water. In the model space, $H_2S(g)$ is supplied continuously from one boundary through convection, allowed to exchange with water films and be oxidized in solution to sulfate, with fractionation factors assigned to each process. Details of the model are provided in the Supplementary Materials.

Interestingly, the model simulations suggest that considerable gradients in sulfate $\delta^{34}S$ occur over meter-scale distances through both gas-water exchange and H_2S

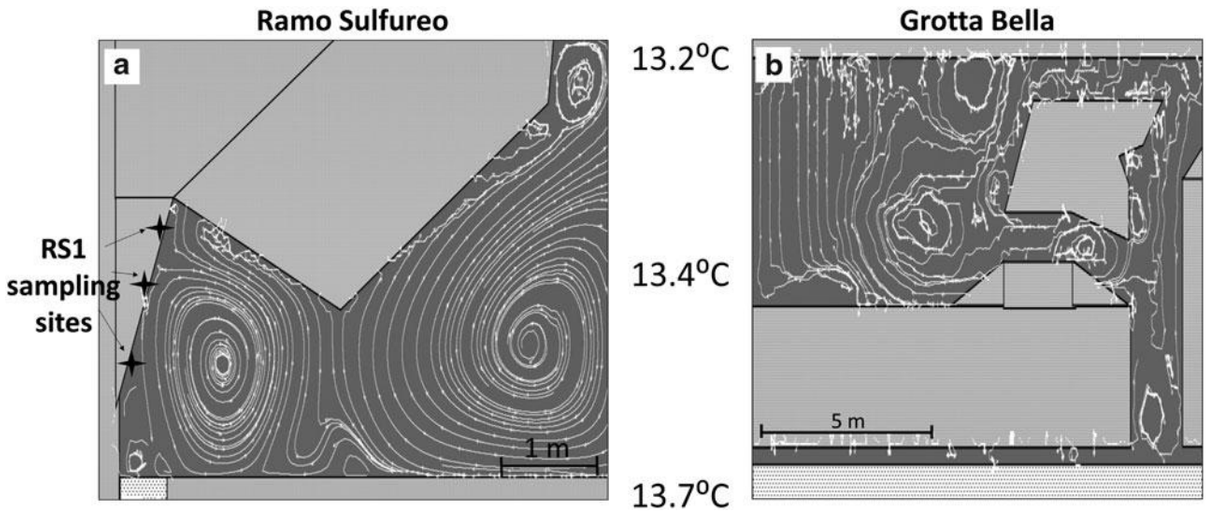

FIG. 6. Snapshots of Energy 2D simulations showing air flow patterns at (**a**) Ramo Sulfureo and (**b**) Grotta Bella due to temperature differences of 0.5°C between bottom and top. In Ramo Sulfureo, large convection cells appear. In Grotta Bella, gas rises upward from the stream and flows through the chimneys. Small convection cells may also appear transiently in both cave rooms.

oxidation. Gas-water exchange imparts transient gradients that disappear on timescales of minutes (Supplementary Fig. S3). Because gypsum formation likely occurs over timescales of weeks to months (Galdenzi and Maruoka, 2003; Jones *et al.,* 2015; Harouaka *et al.,* 2016), gas-water exchange is unlikely to be a primary control on gypsum $\delta^{34}S$. By comparison, H_2S oxidation imparts isotopic gradients that persist at steady state. Depending on the values chosen for the fractionation factor and sulfide oxidation rates, the $\delta^{34}S$ of sulfate (and, by extension, gypsum) can differ by as much as 15‰ over 3 m (Fig. 7). Because of the small volumes of water per unit area at the cave wall-atmosphere interface (width = 0.01 cm; Dreybrodt *et al.,* 2005) and the resulting mass balance of H_2S between gas and aqueous phases, local concentration gradients in the atmosphere (within ~0.5 cm of the interface) are sufficient to generate sizable isotopic effects discernible by meter-scale sampling of gypsum.

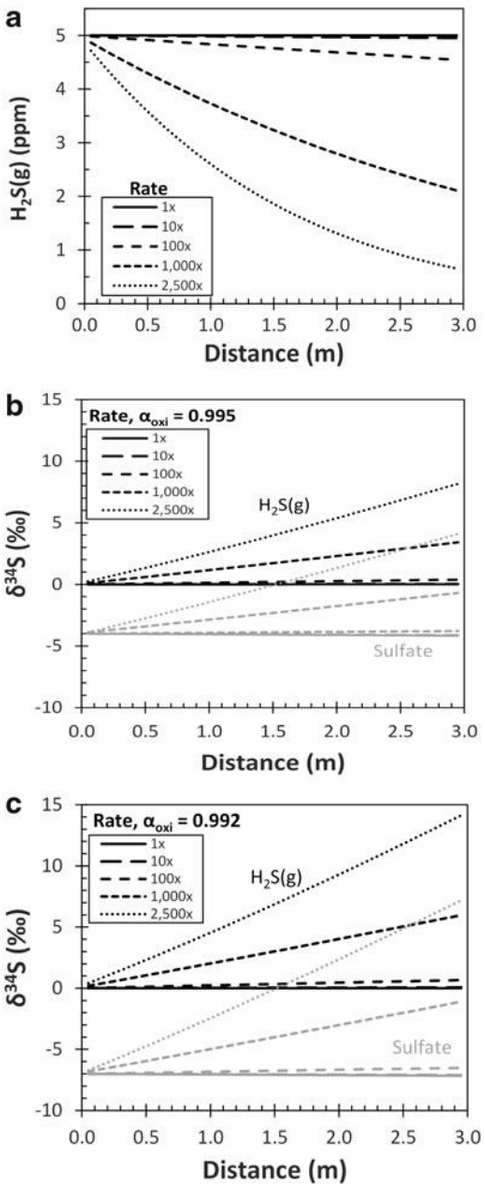

FIG. 7. Results of reactive-transport model at flow rate of 0.2 cm/s, $\alpha_{equi} = 1.001$ and variable oxidation rates. Baseline oxidation rate (1×) was calculated using the abiotic rate law of Millero *et al.* (1987). Faster oxidation rates were tested to simulate microbial H_2S oxidation by changing the abiotic rate constant to be between 10 and 2500 times larger. (**a**) Gas concentration profiles at steady state at various oxidation rates. (**b**) The $\delta^{34}S$ values of $H_2S(g)$ (black lines) and sulfate (gray lines) at various oxidation rates with $\alpha_{oxi} = 0.995$. (**c**) Similar to previous, except $\alpha_{oxi} = 0.992$. Larger isotopic gradients are observed for $H_2S(g)$ and sulfate.

The 1D model is also useful for constraining sulfide oxidation rates, which can provide additional evidence for the importance of microbial H_2S oxidation to gypsum formation. Assuming a constant gas flow velocity and direction, oxidation rates are estimated to be between 0.14 and 0.71 μmol sulfide/m^2/h at site RS1, which are 1000 to 5000 times faster relative to the abiotic rate (Fig. 5). Similar isotopic gradients could be expressed at slower oxidation rates if the actual $H_2S(g)$ flow path is longer, as might be the case for molecules of gas in circulating convection cells. Therefore, the rates determined should be considered as maximum estimates. Our finding implicates microbial H_2S oxidation as an important process in gypsum formation.

Ultimately, we suggest that the isotopic signal of microbial sulfide oxidation is expressed spatially at a meter scale. The spatial pattern differs within a cave room as driven by geometrical variations and patterns of air circulation affected by temperature and pressure. Along a gas flow path, systematic variations of gypsum $\delta^{34}S$ at the meter scale are a potential biosignature, given that slow abiotic oxidation cannot produce the same signal in gypsum deposits.

5.3. Strategies for sampling in cave systems and potential complications

Our observations from actively forming sulfidic cave rooms suggest that systematic variations of gypsum $\delta^{34}S$ along gas flow paths can be interpreted as strong evidence for biosignatures. We therefore propose the following steps to develop sampling strategies in ancient cave systems. Sampling missions should start with reconnaissance and cross-section mapping of a cave room, taking particular note of features where gas may have circulated such as chimneys, rounded domes, and cupolas (Galdenzi and Maruoka, 2003; Audra *et al.,* 2007; De Waele *et al.,* 2016). Visualization of gas flow patterns can be aided with simulations (such as Energy2D), which also allows for some constraints on the flow velocity. Sampling areas within a cave room can then be decided based on the gas circulation patterns. We suggest sampling over certain length spacing/scales where gypsum $\delta^{34}S$ should vary by more than typical analytical $\delta^{34}S$ resolution of < ±0.5‰. The length scale varies as a function of the ratio of H_2S oxidation rate to gas flow velocity but is relatively insensitive to the isotopic fractionation associated with H_2S oxidation (Fig. 8). At high oxidation rate relative to flow velocity, the sampling length scale is <1 m and is easily achievable in many cave rooms. At low oxidation rate to flow velocity, however, the sampling

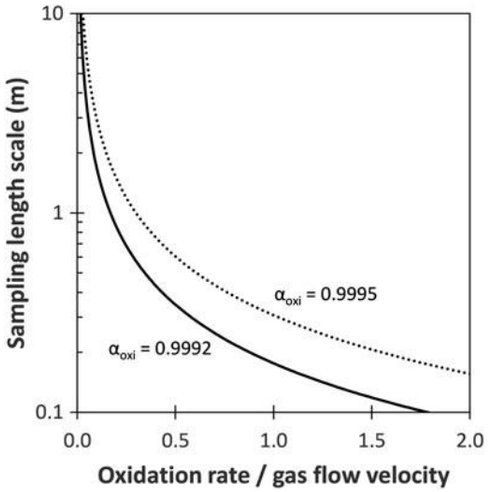

FIG. 8. Sampling length scales at different ratios of H_2S oxidation rate (μmol/m^2/h) to gas flow velocity (cm/s). The length scale here is defined as the minimum sampling spacing required in order to detect gypsum with $\delta^{34}S$ difference of $\geq \pm 0.5‰$, considered as a minimum estimate for analytical resolution. Solid and dashed lines represent simulations where $\alpha_{oxi} = 0.9992$ and 0.9995, respectively.

length scale becomes large (>1 m) and may not be feasible in certain study sites.

Complications with this sampling approach result from uncertainties caused by potential inversions of gas flow as a result of diurnal and seasonal variations, especially for cave rooms located very close to openings to the surface (De Freitas, 1982; Lacanette *et al.,* 2009). Spatial patterns built up in gypsum $\delta^{34}S$ during a particular time period may be overprinted in the subsequent time period. Furthermore, wall gypsum is known to fall to the floor, where it can remain as floor deposits or be dissolved by undersaturated groundwater (*e.g.*, Galdenzi and Maruoka, 2003; De Waele *et al.,* 2016); consequently, any context for spatial pattern is lost.

Additionally, cave gypsum deposits are subjected to recrystallization that can potentially alter their original isotopic compositions (Galdenzi and Maruoka, 2003). Where $H_2S(g)$ is undetectable, Frasassi gypsum deposits tend to be isotopically heavier relative to modern-day groundwater H_2S (−7.5 to −16‰ versus −13 to −21‰; this study; Galdenzi and Maruoka, 2003; Zerkle *et al.,* 2016). One explanation is that old gypsum deposits could be sourced from past groundwater H_2S with higher $\delta^{34}S$. Zerkle *et al.* (2016), however, showed that $\delta^{34}S$ values of groundwater H_2S within a cave room varied by <2‰ over decadal timescales, making this explanation unlikely. Changes over longer timescales remain unconstrained and are not testable with current techniques. Alternatively, as the water table recedes, older gypsum deposits could have been exposed more and more to small quantities of residual $H_2S(g)$ that have higher $\delta^{34}S$ values due to isotopic distillation by extensive sulfide oxidation near the water table. Instead of a H_2S source, older gypsum deposits could also reflect a component of gypsum precipitated from sulfate with high $\delta^{34}S$, which originated from sulfate-reducing microbes (Galdenzi and Maruoka, 2003) or percolating drip waters (Wynn *et al.,* 2013). Regardless of the mechanism (or mechanisms), there are potentials for biogenic signals to be overprinted with time. Sampling missions should thus focus on targeting gypsum deposits that remain on the cave wall and do not show evidence of recrystallization or dissolution.

In summary, gypsum in sulfidic cave rooms displays clear biosignatures for S-oxidizing microbes in the form of systematic $\delta^{34}S$ variations along gas flow paths. We propose strategies for detecting biosignatures in caves as well as other partially enclosed systems by first reconstructing gas flow patterns to decide on sampling areas followed by sampling over a defined length scale. Systematic patterns of gypsum $\delta^{34}S$ along gas flow paths can be considered direct evidence for biological sulfide oxidation. Complications can arise as a result of gas flow inversions and physical or chemical diagenesis that can overprint this biosignature. Constraining these complicating factors should be subjects for future studies.

Acknowledgments

This work was supported by grants to M.S.F. and J.L.M. from NASA NAI (NNA09DA76A and NNA04CC06A). M.M. acknowledges support from the Lewis and Clark Fund for Exploration and Field Research in Astrobiology through NASA and the American Philosophical Society. The authors thank M. Arthur and A. Montanari for providing facilities and laboratory space at Penn State University and the Osservatorio Geologico di Coldigioco in Italy, respectively. Thanks to S. Mariani, S. Cerioni, M. Mainiero, F. Baldoni, S. Carnevali, members of the Gruppo Speleologico C.A.I. di Fabriano and the Federazione Speleological Marchigiana for assistance during field campaigns, and to J. Wang, A. Chorney, Y. Watanabe, L. Liermann, D. Walizer, and I. Schaperdoth for technical support and assistance with laboratory analyses. The authors thank A. Zerkle and an anonymous reviewer for constructive reviews that improved the manuscript.

Author Disclosure Statement

No competing financial interests exist.

References

Audra, P., Hoblea, F., Bigot, J.Y., and Nobecourt, J.C. (2007) The role of condensation-corrosion in the thermal speleogenesis: study of a hypogenic sulfidic cave in Aix-les-Bains, France. *Acta Carsologica* 36:185–194.

Banfield, J.F., Moreau, J.W., Chan, C.S., Welch S.A., and Little, B. (2001) Mineralogical biosignatures and the search for life on Mars. *Astrobiology* 1:447–465.

Bosshard, P.P., Stettler, R., and Bachofen, R. (2000) Seasonal and spatial community dynamics in the meromictic Lake Cadagno. *Arch Microbiol* 174:168–174.

Boston, P.J., Hose, L.D., Northup, D.E., and Spilde, M.N. (2006) The microbial communities of sulfur caves: a newly appreciated geologically driven system on Earth and potential model for Mars. *Geological Society of America Special Papers* 404:331–344.

Buisman, C., Ijspeert, P., Janssen, A., and Lettinga, G. (1990) Kinetics of chemical and biological sulphide oxidation in aqueous solutions. *Water Res* 24:667–671.

Chanton, J.P. (2005) The effect of gas transport on the isotope signature of methane in wetlands. *Org Geochem* 36:753–768.

Committee on an Astrobiology Strategy for the Exploration of Mars. (2007) *An Astrobiology Strategy for the Exploration of Mars,* National Academies Press, Washington, DC.

Czarnacki, M. and Hałas, S. (2012) *Ab initio* calculations of sulfur isotope fractionation factor for H_2S in aqua–gas system. *Chem Geol* 318–319:1–5.

Davis, R. (1958) Displacement reactions at the sulfur atom. I. An interpretation of the decomposition of acidified thiosulfate. *J Am Chem Soc* 2474:3565–3569.

De Freitas, C.R. (1982) Cave climate: assessment of airflow and ventilation. *Int J Climatol* 2:383–397.

Des Marais, D.J., Nuth, J.A., Allamandola, L.J., Boss, A.P., Farmer, J.D., Hoehler, T.M., Jakosky, B.M., Meadows, V.S., Pohorille, A., Runnegar, B., and Spormann, A.M. (2008) The NASA Astrobiology Roadmap. *Astrobiology* 8:715–730.

De Waele, J., Audra, P., Madonia, G., Vattano, M., Plan, L., Ilenia, M.D., Bigot, J.-Y., and Nobécourt, J.C. (2016) Sulfuric acid speleogenesis (SAS) close to the water table: examples from southern France, Austria, and Sicily. *Geomorphology* 253:452–467.

Dreybrodt, W., Gabrovšek, F., and Perne, M. (2005) Condensation corrosion: a theoretical approach. *Acta Carsologica* 34:317–348.

Fry, B., Ruf, W., Gest, H., and Hayes, J.M. (1988) Sulfur isotope effects associated with oxidation of sulfide by O_2 in aqueous solution. *Isot Geosci* 73:205–210.

Galdenzi, S. and Maruoka, T. (2003) Gypsum deposits in the Frasassi Caves, Central Italy. *J Caves Karst Stud* 65:111–125.

Galdenzi, S., Cocchioni, M., Morichetti, L., Amici, V., and Scuri, S. (2008) Sulfidic ground-water chemistry in the Frasassi caves, Italy. *J Caves Karst Stud* 70:94–107.

Grasby, S.E., Beauchamp, B., and Bense, V. (2012) Sulfuric acid speleogenesis associated with a glacially driven groundwater system—Paleo-spring ''pipes'' at Borup Fiord Pass, Nunavut. *Astrobiology* 12:19–28.

Harouaka, K., Eisenhauer, A., and Fantle, M.S. (2014) Experimental investigation of Ca isotopic fractionation during abiotic gypsum precipitation. *Geochim Cosmochim Acta* 129: 157–176.

Harouaka, K., Mansor, M., Macalady, J.L., and Fantle, M.S. (2016) Calcium isotopic fractionation in microbially mediated gypsum precipitates. *Geochim Cosmochim Acta* 184: 114–131.

Hill, C.A. (2000) Overview of the geologic history of cave development in the Guadalupe Mountains, New Mexico. *J Caves Karst Stud* 62:60–71.

Hose, L.D. and Macalady, J.L. (2006) Observations from active sulfidic karst systems: is the present the key to understanding Guadalupe Mountain speleogenesis? In *Caves and Karst of Southeastern New Mexico,* edited by L. Land, New Mexico Geological Society Guidebook, 57th Annual Field Conference, New Mexico Geological Society, Socorro, NM, pp 185–194.

Hose, L.D., Palmer, A.N., Palmer, M.V., Northup, D.E., Boston, P.J., and DuChene, H.R. (2000) Microbiology and geochemistry in a hydrogen-sulphide-rich karst environment. *Chem Geol* 169:399–423.

IAEA. (1995) *Reference and Intercomparison Materials for Stable Isotopes of Light Elements,* International Atomic Energy Agency, Vienna.

Jones, D.S. (2011) *Microbial Ecology and Biogeochemistry of Sulfidic Karst Ecosystems,* PhD dissertation, Pennsylvania State University, University Park, PA.

Jones, D.S., Lyon, E.H., and Macalady, J.L. (2008) Geomicrobiology of biovermiculations from the Frasassi cave system, Italy. *J Caves Karst Stud* 70:78–93.

Jones, D.S., Albrecht, H.L., Dawson, K.S., Schaperdoth, I., Freeman, K.H., Pi, Y., Pearson, A., and Macalady, J.L. (2011) Community genomic analysis of an extremely acidophilic sulfur-oxidizing biofilm. *ISME J* 6:1–13.

Jones, D.S., Schaperdoth, I., and Macalady, J.L. (2014) Metagenomic evidence for sulfide oxidation in extremely acidic cave biofilms. *Geomicrobiol J* 31:194–204.

Jones, D.S., Polerecky, L., Galdenzi, S., Dempsey, B., and Macalady, J.L. (2015) Fate of sulfide in limestone aquifers and implications for sulfuric acid speleogenesis (SAS). *Chem Geol* 410:21–27.

Jones, D.S., Schaperdoth, I., and Macalady, J.L. (2016) Biogeography of sulfur-oxidizing *Acidithiobacillus* populations in extremely acidic cave biofilms. *ISME J* 10:2879–2891.

Kamyshny, A., Druschel, G., Mansaray, Z.F., and Farquhar, J. (2014) Multiple sulfur isotopes fractionations associated with abiotic sulfur transformations in Yellowstone National Park geothermal springs. *Geochem Trans* 15, doi:10.1186/1467-4866-15-7.

Kaplan, I.R. and Rafter, T.A. (1958) Fractionation of stable isotopes of sulfur by thiobacilli. *Science* 127:517–518.

Kaplan, I.R. and Rittenberg, S.C. (1964) Microbiological fractionation of sulphur isotopes. *J Gen Microbiol* 34:195–212.

Lacanette, D., Vincent, S., Sarthou, A., Malaurent, P., and Caltagirone, J.P. (2009) An Eulerian/Lagrangian method for the numerical simulation of incompressible convection flows interacting with complex obstacles: application to the natural convection in the Lascaux cave. *Int J Heat Mass Transf* 52: 2528–2542.

Luther, G.W., Findlay, A.J., MacDonald, D.J., Owings, S.M., Hanson, T.E., Beinart, R.A., and Girguis, P.R. (2011) Thermodynamics and kinetics of sulfide oxidation by oxygen: a look at inorganically controlled reactions and biologically mediated processes in the environment. *Front Microbiol* 2: 1–9.

Macalady, J.L., Lyon, E.H., Koffman, B., Albertson, L.K., Meyer, K., Galdenzi, S., and Mariani, S. (2006) Dominant microbial populations in limestone-corroding stream biofilms, Frasassi cave system, Italy. *Appl Environ Microbiol* 72:5596–5609.

Macalady, J.L., Jones, D.S., and Lyon, E.H. (2007) Extremely acidic, pendulous cave wall biofilms from the Frasassi cave system, Italy. *Environ Microbiol* 9:1402–1414.

Millero, F.J., Hubinger, S., Fernandez, M., and Garnett, S. (1987) Oxidation of H_2S in seawater as a function of temperature, pH, and ionic strength. *Environ Sci Technol* 21: 439–443.

Onac, B.P., Hess, J.W., and White, W.B. (2007) The relationship between the mineral composition of speleothems and mineralization of breccia pipes: evidence from Corkscrew Cave, Arizona, USA. *Can Mineral* 45:1177–1188.

Onac, B.P., Sumrall, J., Tămaş, T., Povară, I., Kearns, J., Dârmiceanu, V., Veres, D., and Lascu, C. (2009) The relationship between cave minerals and H_2S-rich thermal waters along the Cerna Valley (SW Romania). *Acta Carsologica* 38:27–39.

Onac, B.P., Wynn, J.G., and Sumrall, J.B. (2011) Tracing the sources of cave sulfates: a unique case from Cerna Valley, Romania. *Chem Geol* 288:105–114.

Pisarowicz, J. (1994) Cueva de Villa Luz – an active case of H_2S speleogenesis. In *Breakthroughs in Karst Geomicrobiology, Colorado Springs, Colorado* pp. 60–62.

Poser, A., Vogt, C., Knöller, K., Ahlheim, J., Weiss, H., Kleinsteuber, S., and Richnow, H.-H. (2014) Stable sulfur and oxygen isotope fractionation of anoxic sulfide oxidation by two different enzymatic pathways. *Environ Sci Technol* 48:9094–9102.

Raab, M. and Spiro, B. (1991) Sulfur isotopic variations during seawater evaporation with fractional crystallization. *Isot Geosci* 86:323–333.

Sarbu, S.M., Kane, T.C., and Kinkle, B.K. (1996) A chemoautotrophically based cave ecosystem. *Science* 272:1953–1955.

Sarbu, S.M., Galdenzi, S., Menichetti, M., and Gentile, G. (2000) Geology and biology of the Grotte di Frasassi (Frasassi caves) in central Italy: an ecological multi-disciplinary study of a hypogenic underground karst system. In *Ecosystems of the World. 30: Subterranean Ecosystems,* edited by H. Wilkens, D.C. Culver, and W.F. Humphreys, Elsevier, Amsterdam, pp 359–378.

Steefel, C.I., Druhan, J.L., and Maher, K. (2014) Modeling coupled chemical and isotopic equilibration rates. *Procedia Earth and Planetary Science* 10:208–217.

van Everdingen, R.O., Shakur, M.A., and Krouse, H.R. (1985) Role of corrosion by H_2SO_4 fallout in cave development in a travertine deposit—Evidence from sulfur and oxygen isotopes. *Chem Geol* 49:205–211.

Vlasceanu, L., Sarbu, S., Engel, A., and Kinkle, B. (2000) Acidic cave-wall biofilms located in the Frasassi Gorge, Italy. *Geomicrobiol J* 17:125–139.

Watanabe, Y., Farquhar, J., and Ohmoto, H. (2009) Anomalous fractionations of sulfur isotopes during thermochemical sulfate reduction. *Science* 324:370–373.

Wilmot, P.D., Cadee, K., Katinic, J.J., and Kavanagh, B.V. (1988) Kinetics of sulfide oxidation by dissolved oxygen. *J Water Pollut Control Fed* 60:1264–1270.

Wynn, P.M., Borsato, A., Baker, A., Frisia, S., Miorandi, R., and Fairchild, I.J. (2013) Biogeochemical cycling of sulphur in karst and transfer into speleothem archives at Grotta di Ernesto, Italy. *Biogeochemistry* 114:255–267.

Xie, C. (2012) Interactive heat transfer simulations for everyone. *The Physics Teacher* 50:237–240.

Zerkle, A.L., Farquhar, J., Johnston, D.T., Cox, R.P., and Canfield, D.E. (2009) Fractionation of multiple sulfur isotopes during phototrophic oxidation of sulfide and elemental sulfur by a green sulfur bacterium. *Geochim Cosmochim Acta* 73:291–306.

Zerkle, A.L., Jones, D.S., Farquhar, J., and Macalady, J.L. (2016) Sulfur isotope values in the sulfidic Frasassi cave system, central Italy: a case study of a chemolithotrophic S-based ecosystem. *Geochim Cosmochim Acta* 173:373–386.

Zhang, J.Z. and Millero, F.J. (1991) The rate of sulfite oxidation in seawater. *Geochim Cosmochim Acta* 55:677–685.

Address correspondence to:
Muammar Mansor
Dept. of Geological Sciences
University of Texas at El Paso
500 W. University Ave
El Paso, TX 79902

E-mail: muammar10@gmail.com

Submitted 17 January 2017
Accepted 9 June 2017

Abbreviations Used

EDS = energy dispersive spectroscopy
GB = Grotta Bella
RS = Ramo Sulfureo
V-CDT = Vienna Canyon Diablo Troilite